

Article

Crystal Structure of New 1-Phenyl-Substituted Tribenzsilatranes

Vitalijs Romanovs ^{1,*}, Sergey Belyakov ^{1,*}, Evgeniya Doronina ² , Valery Sidorkin ^{2,*} , Thierry Roisnel ³ and Viatcheslav Jouikov ³¹ Latvian Institute of Organic Synthesis, Aizkraukles 21, LV-1006 Riga, Latvia² A. E. Favorsky Irkutsk Institute of Chemistry, Siberian Branch of the Russian Academy of Sciences, 1 Favorsky str., 664033 Irkutsk, Russia³ UMR 6226-ISCR, University of Rennes, 35042 Rennes, France; therry.roisnel@univ-rennes1.fr (T.R.); vjouikov@univ-rennes.fr (V.J.)

* Correspondence: vitalijs.romanovs@inbox.lv (V.R.); serg@osi.lv (S.B.); svf@irioc.irk.ru (V.S.)

Abstract: The family of practically requested “common” silatrane derivatives of triethanolamine X-Si(OCH₂CH₂)₃N, **1**, was enlarged with the first representatives of 3,4,6,7,10,11-tribenzo-2,8,9trioxa-5-aza-1-silatricyclo(3.3.3.0^{1,5})undecanes X-Si(O-*para*-R-C₆H₃)₃N, tribenzsilatranes **2** (R = H (**a**), Me (**b**), F (**c**)), carrying the substituent R in the side aromatic rings. These compounds were prepared via the transesterification of phenyl trimethoxysilane with the corresponding triphenol amines and studied using XRD and DFT calculations. These derivatives of 1-X-(4-R-2,2',2''-nitriolotriphenoxy)silane are expected to have, as their parent “common” silatranes **1**, diverse biological and pharma activities. A common characteristic feature of the molecular structures of both **1** and **2** is the presence of an intramolecular dative bond N→Si whose existence is evidenced by geometric and quantum topological (AIM) criteria. In the crystals, the length of this bond (*d*_{SiN}) is noticeably longer in tribenzsilatranes than in **1**. The results of DFT B3PW91/6-311++G(d,p) calculations suggest the reason for this to be the more rigid nature of the potential functions of the N→Si bond deformation in **2** compared to **1**. The relative degree of “softness”/“hardness” of the potential functions can be assessed from the difference in the calculated values of *d*_{SiN} in isolated molecules **1** and **2a–c** and in their crystals.

Keywords: silatranes; tribenzsilatranes; crystal structure analysis; intramolecular dative bonds

Citation: Romanovs, V.; Belyakov, S.; Doronina, E.; Sidorkin, V.; Roisnel, T.; Jouikov, V. Crystal Structure of New 1-Phenyl-Substituted Tribenzsilatranes. *Crystals* **2023**, *13*, 772. <https://doi.org/10.3390/cryst13050772>

Academic Editor: Thomas M. Klapötke

Received: 1 April 2023

Revised: 29 April 2023

Accepted: 4 May 2023

Published: 6 May 2023



Copyright: © 2023 by the authors. Licensee MDPI, Basel, Switzerland. This article is an open access article distributed under the terms and conditions of the Creative Commons Attribution (CC BY) license (<https://creativecommons.org/licenses/by/4.0/>).

1. Introduction

The most remarkable specificity of “common” silatranes X-Si(OCH₂CH₂)₃N (**1**) is a dative bond between the nitrogen atom and silicon, which predetermines their unique structure, unusual spectral characteristics and reactivity, as well as a wide range of biological activity [1–6]. Moreover, experimental and theoretical studies of **1** indicate the extreme softness of the potential functions of deformation of the N→Si bond [6–10]. According to high-precision CCSD(T) calculations, only ca. 0.02 eV is needed to modify the Si···N distance by as much as 0.1 Å [9]. As a result, silatranes **1** have a characteristic feature: hypersensitivity to internal (nitrogen environment) and external (phase state, solvent, temperature) factors [1,2,6–10]. For instance, the Si···N contact length in X-Si(OCH₂CH₂)₃N (X = H, Me, F) in the gas phase, according to electron diffraction data and the results of quantum chemical calculations, exceeds the corresponding value in the crystalline phase (from XRD) by more than 0.25 Å [1,7,10–14].

Upon substitution of lateral ethylene chains in **1** for phenylene fragments (i.e., going to tribenzsilatranes X-Si(OC₆H₄)₃N (**2**)), a noticeable elongation of the Si···N contact is observed (according to XRD data [2,15–17]). This elongation can be related to the increased rigidity of the atrane cage (in other words, to the profile of the potential function of deformation of the N→Si bond).

As an alternative explanation, the redistribution of electronic effects in the side chains (substitution of alkane carbon atoms for more electronegative aromatic ones) can also be advanced [17]. However, neither of these explanations have yet received convincing support. It is also important to emphasize that of the five known tribenzsilatranes **2** ($X = \text{Cl}$, CH_2Cl , Ph , $\text{Si}(\text{SiMe}_3)_3$ and $\text{Si}(\text{SiMe}_3)_2\text{SiMe}_2\text{SiMe}_2\text{Si}(\text{SiMe}_3)_3$) [15–17], there is not a single structure bearing the substituents in the side phenylene groups. Meanwhile, preparing such derivatives and studying them by means of X-ray diffractometry and quantum chemistry could undoubtedly contribute to a deeper understanding of the role played by electronic and steric effects in the formation of the atrane backbone of molecules **2** and, thus, to their more meaningful and efficient practical use.

In this regard, we realized the synthesis of the derivatives of 1-phenyl-tribenzsilatranes $\text{Ph-Si}(\text{O-para-R-C}_6\text{H}_3)_3\text{N}$ **2** ($R = \text{H}$, Me , F), carried out their X-ray diffraction analysis and the related quantum chemical calculations.

2. Materials and Methods

2.1. Single Crystal X-ray Diffraction

The X-ray diffraction data for compounds of **2a** ($R = \text{H}$), **2b** ($R = \text{Me}$) and **2c** ($R = \text{F}$) were collected on automatic four-circle diffractometers (Bruker-AXS GmbH, Champs-sur-Marne, France), D8 VENTURE Bruker AXS and APEXII Kappa-CCD (Bruker-AXS), using molybdenum monochromatic $\text{Mo-K}\alpha$ radiation ($\lambda = 0.71073 \text{ \AA}$).

2.2. Modeling and Quantitative Analysis of Crystal Structures

The crystal structures were determined through direct methods with the *SHELXT* [18] structure solution program using Intrinsic Phasing and refined with the *SHELXL* refinement package [19].

For the structures with good R-factors (**2b** and **2c**), H atoms were partly localized from Fourier difference series and on the basis of the geometrical considerations. The positions of H atoms were refined within the riding model (refining the C atom carrying the given H atom at a constant C-H distance).

2.3. Computational Details

Optimization of the structure of isolated molecules of 1-phenylsilatrane **1** and 1-phenyl-tribenzsilatranes **2a–c** was carried out through the density functional theory method DFT B3PW91/6-311++G(d,p). The literature [10] attests that this method perfectly reproduces the known experimental gas-phase (electron diffraction) geometries of “common” silatranes $\text{X-Si}(\text{OCH}_2\text{CH}_2)_3\text{N}$ ($X = \text{H}$, Me , F). The value of the mean arithmetic error (MAE = 0.02) when using the B3PW91 method for describing the $\text{Si} \cdots \text{N}$ contact length in these compounds suggests that this method is almost as good as high-precision CCSD due to the lucky compensation of errors.

The optimized structures corresponded to the minima on the potential energy surface, as was confirmed by the positive eigenvalues of the corresponding Hessians.

The calculations were performed using the package Gaussian 09 [20].

The analysis of the MP2(full)/6-311++G(d,p) electron distribution of $\rho(\mathbf{r})$ in **1**, **2a–c** was performed with the atoms-in-molecules (AIM) approach [21], using the AIMALL program [22]. AIM estimation of the energy [23–26] of dative contact $\text{N} \rightarrow \text{Si}$ (E_{SiN}) was performed according to the well-proven [27–35] relation $E_{\text{SiN}} = -V(\mathbf{r}_c)/2$, with $V(\mathbf{r}_c)$ being the potential energy density at the bond critical point $\text{bcp}(\text{SiN})$. Natural bond orbital (NBO) [36] analysis was performed using the NBO program NBO 5.0 [37] via the interface FIREFLY [38] on HF/6-311++G(d,p) molecular orbitals.

The degree of pentacoordination of silicon (η_e) in **2a–c** was calculated using Tamao’s

formula: $\eta_e = \left(1 - \frac{120 - 1/3 \sum_{n=1}^3 \varphi_n}{120 - 109.5}\right) \times 100\%$ (φ is the angle between the equatorial bonds to Si) [39].

2.4. Synthesis of the Compounds

The title tribenzsilatranes were prepared through the transesterification of commercially available phenyl trimethoxysilane. The reaction requires the use of dibutyl ether (*n*-Bu₂O), a polar yet non-coordinating solvent, because the starting triphenolamines easily coordinate with solvents such as dimethylformamide to form, along with some amount of the desired product, a dimethylformamide-coordinated amine that crystallizes during the workup. The progress of the reaction was monitored through TLC. After synthesis, the products were rinsed with pentane and purified through a celite/activated-carbon filter, then recrystallized from carbon tetrachloride.

1-Ph Tribenzsilatrane (**2a**) was prepared in 58% yield as described in [40] and had identical physical constants. The syntheses of tribenzsilatranes **2b** and **2c** followed the same protocol, i.e., heating the mixture of the amine (1 eq.) and the trialkoxysilane (1.3 eq.) for 18 h at 130 °C in an inert argon atmosphere. Dry dibutyl ether (distilled prior to use from sodium benzophenone ketyl) was used as a solvent. After cooling down to room temperature, the solid was filtered off, rinsed with pentane, purified through a carbon–celite filter and then recrystallized from carbon tetrachloride to give monocrystalline material suitable for XRD. In total, three tribenzsilatranes were synthesized with good yields (58–80%).

1-Ph *p*-Me-tribenzsilatrane (**2b**). The mixture of the triphenolamine (0.10 g, 0.30 mmol) and the trialkoxysilane (0.09 mL 0.39 mmol) was heated for 18 h at 130 °C in an argon atmosphere. Dry dibutyl ether was used as a solvent. The formed solid was filtered off, washed with pentane, then dissolved in a minimal amount of CH₂Cl₂ to be purified through a carbon–celite filter, and then recrystallized from carbon tetrachloride to give the desired compound **2b** as colorless needles (0.08 g, 63%).

¹H NMR: (400 MHz, CDCl₃) δ_H: 8.12–8.05 (m, 2H), 7.68 (d, *J* = 8.1 Hz, 3H), 7.54–7.47 (m, 3H), 6.92 (d, *J* = 2.0 Hz, 3H), 6.79 (dd, *J* = 8.2, 1.9 Hz, 3H), 2.28 (s, 9H). ¹³C NMR: (101 MHz, CDCl₃) δ_C: 153.2, 139.4, 135.0, 134.5, 129.7, 127.8, 125.4, 122.9, 118.4, 21.4. Anal. calcd. for C₂₇H₂₃NO₃Si: C, 74.11; H, 5.30; N, 3.20. Found: C, 74.38; H, 5.34; N, 3.66.

1-Ph *p*-F-tribenzsilatrane (**2c**). The mixture of the amine (0.15 g, 0.43 mmol) with the trialkoxysilane (0.13 mL, 0.56 mmol) in dry dibutyl ether was heated for 18 h at 130 °C under argon. After the reaction was over, the solid was filtered off, rinsed with pentane, purified through a carbon–celite filter and then recrystallized from carbon tetrachloride to give the desired benzsilatrane **2c** as green needles (0.17 g, 80%).

¹H NMR: (400 MHz, CDCl₃) δ_H: 8.07–7.97 (m, 2H), 7.69 (dd, *J* = 8.8, 5.6 Hz, 3H), 7.54–7.46 (m, 3H), 6.82 (dd, *J* = 9.3, 2.8 Hz, 3H), 6.72 (m, *J* = 8.8, 8.2, 2.9 Hz, 3H). ¹³C NMR: (101 MHz, CDCl₃) δ_C: 134.9, 128.0, 127.0, 126.9, 109.8, 109.5, 106.2, 105.9. Anal. calcd. for C₂₄H₁₄F₃NO₃Si: C, 64.14; H, 3.14; N, 3.12. Found: C, 64.33; H, 3.27; N, 3.54.

3. Results

3.1. Crystal Structure of **2a–c**

The main crystal data for the three prepared phenyl tribenzsilatranes are listed in Table 1.

Figure 1 shows a perspective view of molecules **2a–c** with thermal ellipsoids, and the atom numbering scheme follows in the text. The crystal structure of **2a** has been described in [15]. These crystals of **2a** belong to the rhombic pyramidal crystal class (space group *Cmc*2₁). In the crystal structure, molecules **2a** lie in the special positions (in mirror symmetry planes *m*). Therefore, atoms Si1, O2, C3, C4, N5, C12, C15, C18, C19, C20 and C21 are in these planes. Figure 2 illustrates a fragment of the molecular packing of **2a**, revealing C–H···π interactions that were not described in the earlier work [15]. In this crystal structure, the C14–H group (as well as the symmetrically equivalent C16–H group) forms an intermolecular hydrogen bond of the CH···π type with the aromatic ring. The geometric parameters of this bond are as follows: C···C_g (−*x* + $\frac{1}{2}$, −*y* + $\frac{1}{2}$, *z* − $\frac{1}{2}$) = 3.673(15) Å, H···C_g = 2.88 Å, C–H···C_g = 144°, where C_g is the centroid of ring C6–C7–C25–C24–

C23–C22. By means of these bonds, the molecular layers are formed in the crystal structure. These layers are located in an arrangement parallel to the glide symmetry plane *c*.

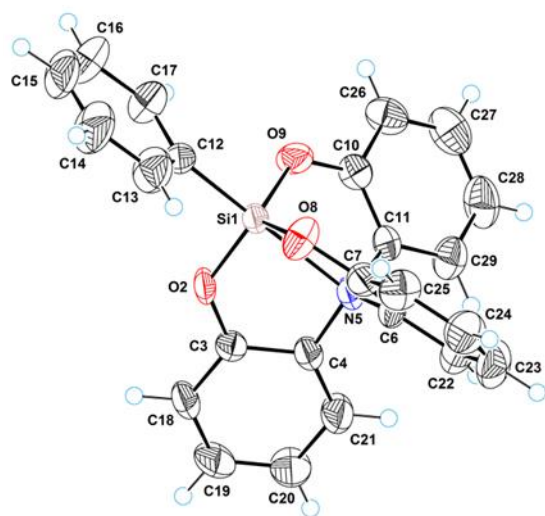
Table 1. Crystal data and structure refinement parameters for **2a–c**.

Parameter	2a	2b	2c
Empirical formula	C ₂₄ H ₁₇ NO ₃ Si	C ₂₇ H ₂₃ NO ₃ Si	C ₂₄ H ₁₄ F ₃ NO ₃ Si
Formula weight, <i>M_r</i>	395.47	437.55	449.45
Temperature (K)	296(2)	150(2)	150(2)
Diffractometer	D8 VENTURE	APEXII	APEXII
	Bruker AXS	Bruker AXS	Bruker AXS
Crystal size (mm ³)	0.80 × 0.36 × 0.27	0.33 × 0.24 × 0.10	0.58 × 0.42 × 0.09
Crystal system	orthorhombic	monoclinic	monoclinic
Space group	<i>Cmc</i> 2 ₁	<i>P</i> 2 ₁ / <i>c</i>	<i>P</i> 2 ₁ / <i>n</i>
<i>a</i> (Å)	11.127(6)	10.086(1)	9.571(2)
<i>b</i> (Å)	14.714(4)	12.433(1)	12.308(2)
<i>c</i> (Å)	11.892(3)	19.107(2)	17.430(2)
β (°)	90	104.594(6)	91.533(5)
Unit cell volume (Å ³)	1946.9(13)	2318.7(4)	2052.5(5)
Molecular multiplicity	4	4	4
Absorption coefficient (mm ^{−1})	0.147	0.130	0.169
<i>F</i> (000)	824	920	920
Calculated density (g/cm ³)	1.349	1.253	1.454
2θ _{max} (°)	55.0	51.0	55.0
Reflections collected	6266	15,749	11,432
Independent reflections with <i>I</i> > 2σ(<i>I</i>)	1901	2351	3348
Number of refined parameters	137	292	289
<i>R</i> -factor	0.1105	0.0636	0.0417
CCDC number	2247806	2247803	2247804

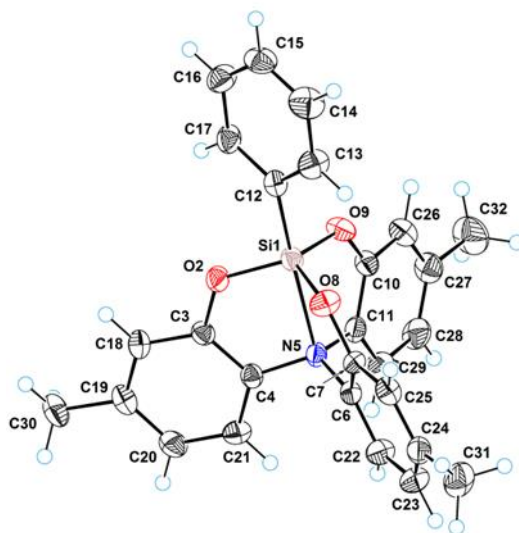
An interesting feature of the molecular packing of **2a** is that it almost lacks voids in its crystal structure. In fact, only small cavities were revealed in the crystal structure. These cavities are located practically on the screw axes of symmetry 2₁ and, thus, are repeated through half of the translation along the crystallographic axis *c* (see Figure S1 Supplementary Materials). The total volume of these cavities in the unit cell amounts to 18.6 Å³. Such a small volume of the voids leads to the fact that the density of **2a** is relatively high (*d* = 1.349 g/cm³).

The crystal structures of **2b** and **2c** are drastically different from **2a**. The crystals of **2b** and **2c** belong to the prismatic crystal class 2/*m*. In these crystals, molecules **2b** and **2c** lie in general positions. The crystal structure of **2b** also contains C–H···π interactions similar to the structure **2a**. The C15–H and C16–H groups form such interactions with aromatic rings. These interactions are shown in Figure 3. The geometric parameters of these bond are as follows: C15···Cg1 ($-x + 2, y - \frac{1}{2}, -z + \frac{1}{2}$) = 3.819(5) Å, H···Cg = 3.08 Å, C–H···Cg = 135°; C16···Cg2 ($-x + 2, y - \frac{1}{2}, -z + \frac{1}{2}$) = 3.857(5) Å, H···Cg = 3.09 Å, C–H···Cg = 139°, where Cg1 and Cg2 are the centroids of rings C10–C11–C29–C28–C27–C26 and C3–C4–C21–C20–C19–C18, respectively. Thus, these bonds are weaker than the C–H···π bonds in the **2a** structure, but in **2b**, a pair of neighboring molecules are connected by two such bonds. By means of these bonds, the molecular chains in **2b** are formed along the monoclinic axis.

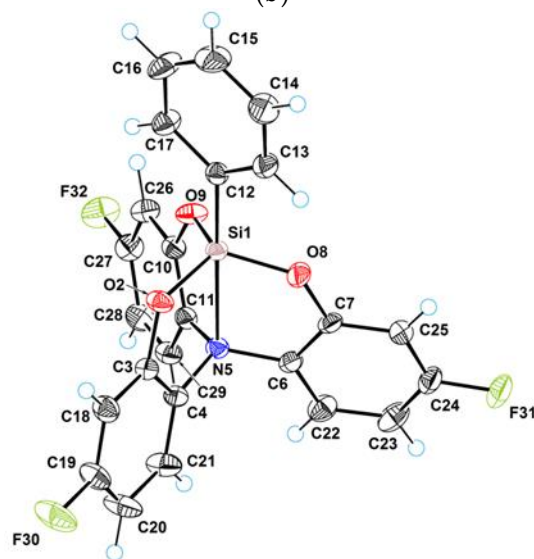
In contrast to **2a**, the volume of voids in the crystal structure of **2b** is quite significant and amounts to 68.4 Å³ in the unit cell. These voids are located in the general positions of the unit cell near the centers of inversion (see Figure S2 Supplementary Materials). The volume of one void region is, thus, 17.1 Å³, which corresponds to the volume of small molecules (such as water). However, due to the fact that substance **2b** is hydrophobic, crystal hydrates have not been formed. The presence of the relatively large cavities leads to a decrease in the density of **2b** (*d* = 1.253 g/cm³) in comparison with **2a**.



(a)



(b)



(c)

Figure 1. ORTEP diagram for molecules 2a (a), 2b (b) and 2c (c) showing atomic labels and 50% probability displacement ellipsoids. Hydrogen atoms are shown as small spheres of arbitrary radii.

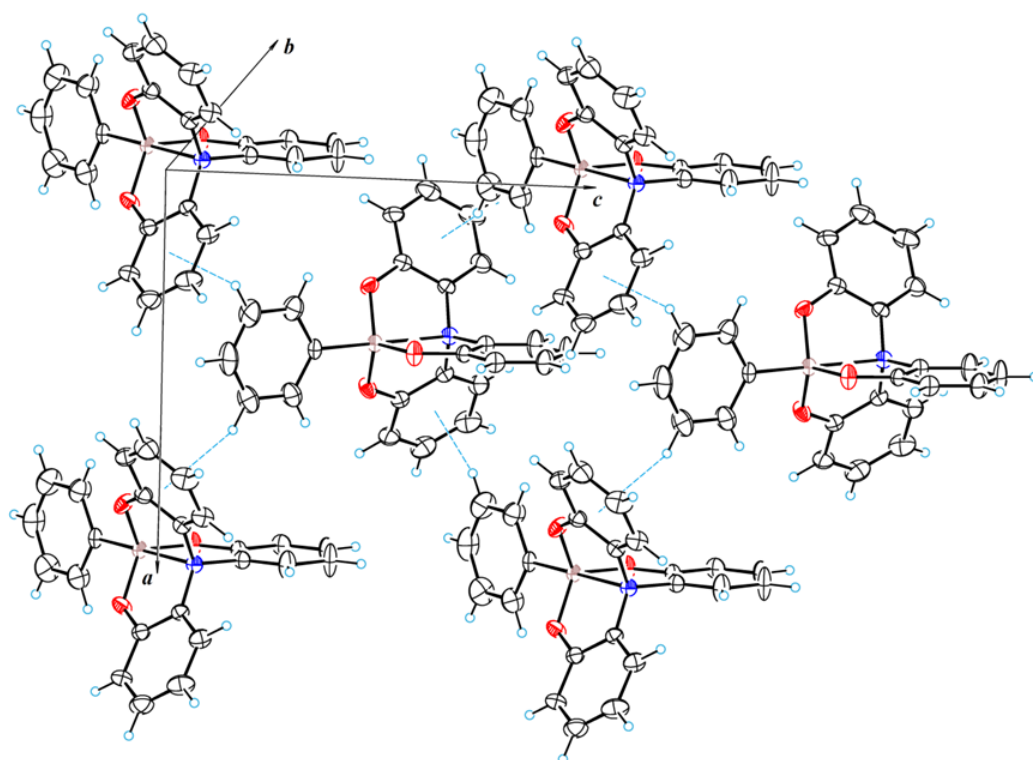


Figure 2. Part of the crystal structure of **2a**, showing the formation of a layer built with $\text{CH} \cdots \pi$ hydrogen bonds. Hydrogen atoms are shown as small spheres of arbitrary radii.

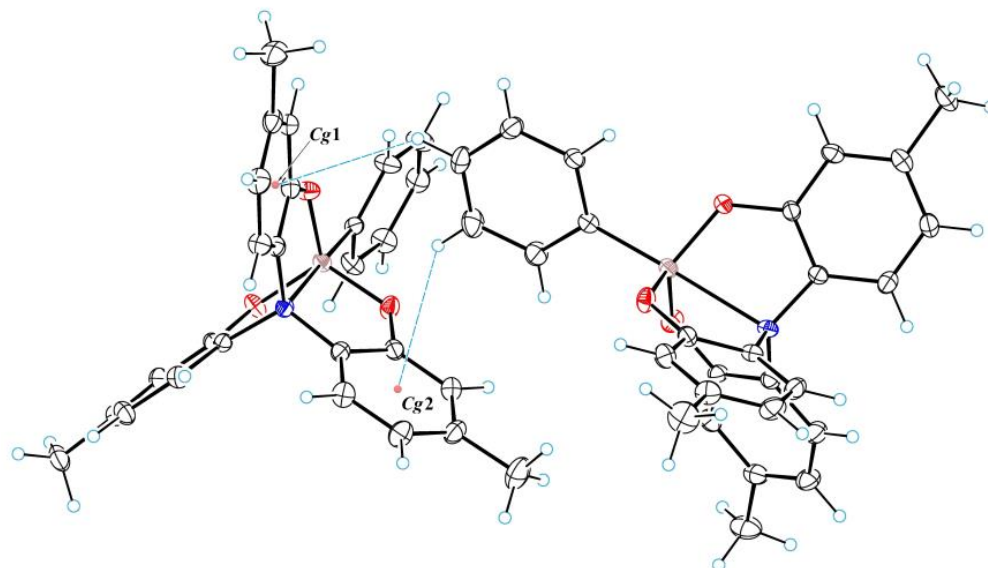


Figure 3. $\text{CH} \cdots \pi$ hydrogen bonds in the crystal structure **2b**.

In the crystal structure of **2c**, the strongest intermolecular interactions are due to fluorine atoms. These contacts are depicted in Figure 4 (dotted lines). The interactions $\text{F30} \cdots \text{H-C15}(x, y - 1, z)$ and $\text{F32} \cdots \text{H-C23}(x - \frac{1}{2}, -y + \frac{1}{2}, z - \frac{1}{2})$ can be described as hydrogen bonds of the $\text{CH} \cdots \text{F}$ type. The parameters of these bond are as follows: $\text{F30} \cdots \text{C15} = 3.257(2) \text{ \AA}$, $\text{F} \cdots \text{H} = 2.90 \text{ \AA}$, $\text{C-H} \cdots \text{F} = 104^\circ$; $\text{F32} \cdots \text{C23} = 3.167(2) \text{ \AA}$, $\text{F} \cdots \text{H} = 3.12 \text{ \AA}$, $\text{C-H} \cdots \text{F} = 84^\circ$. The third interaction of the $\text{F} \cdots \pi$ type is $\text{F31} \cdots \text{Cg}(x - 1, y, z)$, where Cg is the centroid of the ring C12–C13–C14–C15–C16–C17. The distance $\text{F31} \cdots \text{Cg}$ amounts to $3.180(2) \text{ \AA}$. Due to these intermolecular interactions, the crystal structure of **2c** forms a three-dimensional molecular framework.

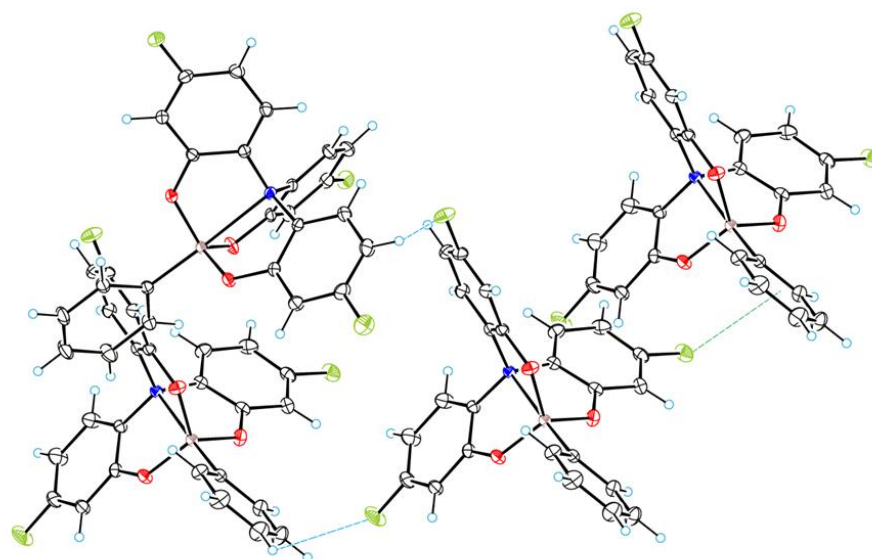


Figure 4. Intermolecular interactions involving fluorine atoms in the crystal structure **2c**.

The presence of this kind of interaction in the crystal cell **2c** is also supported by quantum topological AIM analysis (see Figure S3 Supplementary Materials), detecting $bcp(3, -1)$ critical points in the corresponding inter-atomic regions $F \cdots H$ and $F \cdots C$.

In the structure of **2c**, the voids occupy a smaller volume compared to **2b** (see Figure S4 Supplementary Materials), which is still larger than in **2a**. Their total volume per unit cell is 39.6 \AA^3 , which leads to an increase in the density of the substance in comparison with **2b**. Considering that in the molecular structure of **2c**, instead of hydrogen atoms, there are three fluorine atoms, which have a Van der Waals radius close to that of hydrogen but are 19 times heavier than hydrogen, the compound **2c** has the highest density of the three tribenzsilatranes studied ($d = 1.454 \text{ g/cm}^3$).

3.2. Geometry of Silatrane Cage in **2a–c**

Table 2 (for more complete data, see Table S1 Supplementary Materials) presents selected bond lengths and angles characterizing the geometry of the silatrane cage in tribenzsilatranes **2**. The common characteristic feature of their molecular structure is the presence of an intramolecular donor–acceptor bond $N \rightarrow Si$. Its existence is evidenced by both geometric (the length of the $Si \cdots N$ contact is less than the sum of the Van der Waals radii of Si and N atoms, 3.65 \AA) and by quantum topological (AIM) criteria (the presence of a bond critical point $(3, -1)$ in the inter-atomic region $Si \cdots N$, see Figure 5).

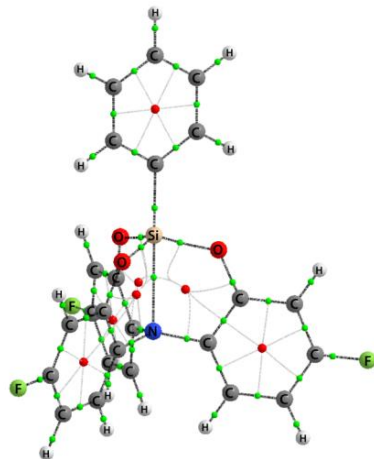


Figure 5. MP2(full)/6-311++G(d,p) molecular graph of **2c**. The small green spheres represent the $bcp(3, -1)$ bond critical points, and the red spheres represent ring critical points $rcp(3, 1)$.

Table 2. XRD Experimental and B3PW91/6-311++G(d,p) calculated (*italics*) selected geometric parameters of molecules **2a–c** (bond lengths in Å, angles in °).

Parameter	2a		2b		2c	
	exp.	<i>calc.</i>	exp.	<i>calc.</i>	exp.	<i>calc.</i>
Si1–O2	1.654(8)	<i>1.681</i>	1.657(2)	<i>1.684</i>	1.655(2)	<i>1.683</i>
Si1–C12	1.863(11)	<i>1.861</i>	1.850(3)	<i>1.863</i>	1.852(3)	<i>1.857</i>
O2–C3	1.342(14)	<i>1.353</i>	1.370(4)	<i>1.353</i>	1.369(4)	<i>1.349</i>
C3–C4	1.400(15)	<i>1.399</i>	1.387(4)	<i>1.398</i>	1.392(4)	<i>1.400</i>
N5–C4	1.443(13)	<i>1.438</i>	1.446(4)	<i>1.440</i>	1.444(4)	<i>1.437</i>
O2–Si1–O8	117.1(3)	<i>115.0</i>	116.0(1)	<i>115.4</i>	116.2(1)	<i>114.7</i>
O2–Si1–C12	100.3(4)	<i>102.1</i>	98.9(1)	<i>102.2</i>	102.5(1)	<i>103.2</i>
Si1–O2–C3	126.3(7)	<i>126.4</i>	125.7(2)	<i>126.1</i>	125.9(2)	<i>126.8</i>
O2–C3–C4	118.2(11)	<i>119.7</i>	118.1(3)	<i>119.6</i>	119.2(3)	<i>120.0</i>
C3–C4–N5	113.3(10)	<i>114.7</i>	113.9(3)	<i>114.8</i>	114.4(3)	<i>115.0</i>
C4–N5–C6	116.5(7)	<i>117.1</i>	114.7(2)	<i>117.3</i>	116.8(2)	<i>117.4</i>
N5–Si1–C12	179.8(4)	<i>179.6</i>	178.2(1)	<i>179.6</i>	178.0(1)	<i>179.5</i>
Si1–N5	2.329(9)	<i>2.463</i>	2.358(3)	<i>2.451</i>	2.411(3)	<i>2.494</i>
ΔN	0.300(9)	<i>0.357</i>	0.292(4)	<i>0.247</i>	0.267(4)	<i>0.230</i>
ΔSi	0.284(7)	<i>0.243</i>	0.286(3)	<i>0.346</i>	0.318(3)	<i>0.372</i>
η_e	72.4	<i>58.4</i>	72.2	<i>60.9</i>	65.8	<i>54.9</i>
$\Sigma(O-Si-O)$	351.4(3)	<i>346.9</i>	351.3(1)	<i>347.7</i>	349.3(1)	<i>345.8</i>
$\Sigma(C-N-C)$	347.4(7)	<i>351.6</i>	348.2(2)	<i>351.3</i>	350.0(2)	<i>352.5</i>

Judging by the properties of the detected $bcp(3, -1)$, the N→Si bond in phenyl tribenzsilatranes **2a–c** (just as in phenylsilatrane **1**) formally belongs to the intermediate type of inter-atomic interactions (Table 3). Indeed, the positive sign of the Laplacian $\nabla^2\rho(\mathbf{r}_c)$ suggests that this bond is ionic, while according to the negative sign of the electron energy density $E(\mathbf{r}_c)$, it is covalent [41,42].

Table 3. Geometric * parameters of the coordination node CSiO₃N and quantum topological ** characteristics at the bond critical point $bcp(SiN)$ of **1** and **2a–c** as isolated molecules and in crystal.

Compound		d_{SiN}	η_e	$\rho(\mathbf{r})$	$\nabla^2\rho(\mathbf{r})$	$E(\mathbf{r}_c)$	E_{SiN}	Ref.	
1	gas	2.515	54	0.235	0.861	−0.07	8.9		
	crystal	α	2.193	86	0.370	1.984	−0.17	22.6	[43]
		β	2.156	87	0.391	2.554	−0.18	25.1	[44]
		γ	2.132	88	0.404	2.908	−0.18	26.7	[45]
2a	gas	2.463	58	0.256	0.737	−0.08	10.2		
	crystal	2.344	72	0.299	0.866	−0.13	14.6	[15]	
		2.329	72	0.311	0.823	−0.14	15.5	this work	
2b	gas	2.451	61	0.261	0.701	−0.09	10.5		
	crystal	2.358	72	0.296	0.745	−0.12	13.9	this work	
2c	gas	2.494	55	0.244	0.786	−0.07	9.4		
	crystal	2.411	66	0.274	0.749	−0.10	11.9	this work	

* Inter-atomic distance Si···N (d_{SiN} , Å) and degree of pentacoordination of silicon (η_e , %). ** Electron density ($\rho(\mathbf{r}_c)$, e/Å³), Laplacian ($\nabla^2\rho(\mathbf{r}_c)$, e/Å⁵), electron energy density ($E(\mathbf{r}_c)$, hartree/Å³) in $bcp(SiN)$ and energy of the dative bond N→Si (E_{SiN} , kcal/mol).

As expected [31–33], the geometric and quantum topological descriptors of the dative bond N→Si of the molecules **2** (as well as **1**) change coherently. For instance, the shortening of the N→Si bond length (d_{SiN}) is accompanied by an increase in the electron density $\rho(\mathbf{r})$ in the corresponding $bcp(SiN)$ and by an increase in the energy of the dative bond N→Si (E_{SiN}) (Table 3).

As noted above (see Introduction), the replacement of ethylene fragments in “ordinary” silatrane **1** (for crystal structure of **1**, see Figure S5 Supplementary Materials) with phenylene fragments (i.e., the transition to tribenzsilatranes **2**) leads to a noticeable elongation (according to XRD data [2]) of the Si···N (d_{SiN}) contact. Moreover, this feature is fundamentally independent of the effect of crystal polymorphism and of the quality of crystals (the magnitude of the R-factor). For instance, for the three polymorph modifications α , β and γ of the “common” phenylsilatrane Ph-Si(OCH₂CH₂)₃N, the Si···N distance is $d_{\text{SiN}} = 2.193$ Å (α) [43], 2.156 Å (β) [44] and 2.132 Å (γ) [45], while for tribenzsilatrane Ph-Si(OC₆H₄)₃N, **2a**, $d_{\text{SiN}} = 2.329$ Å (R-factor = 0.1105, this work) and 2.344 Å (R-factor = 0.0599 [15]). The ratio $d_{\text{SiN}}(\mathbf{1}) < d_{\text{SiN}}(\mathbf{2})$ also holds for tribenzsilatranes **2b,c** containing, in contrast to **2a**, *para*-substituents in the side phenylene groups (see Table 2).

Based on the literature [2,17], this fact can be explained by the relatively high energy requirements, ΔE , for the N→Si bond deformation in **2a–c** compared to those in **1**. Indeed, according to the calculations performed, it takes less energy to shorten the Si···N contact length by 0.1 Å in **1** than in **2** (see Figure 6). With this, it is important to emphasize that, judging by the value of ΔE , the “softness” of the potential function $E = f(d_{\text{SiN}})$ for structures **2a–c** is comparable (Figure S6 Supplementary Materials). This fact does not allow us to explain the observed increase in the solid-phase d_{SiN} in the series **2a**, **2b**, **2c** with confidence. On the other hand, taking the difference in the calculated values of d_{SiN} in isolated molecules **1** and **2a–c** and in crystals, $\Delta d_{\text{SiN}}^{\text{gas-solid}}$ (see Table 2), as a measure of the relative “softness”/“hardness” of potential functions [7,10], one obtains the series $\Delta d_{\text{SiN}}^{\text{gas-solid}}$ (Å): 0.32–0.38 (**1**) > 0.12–0.13 (**2a**) > 0.09 (**2b**) > 0.08 (**2c**) (regardless of the polymorphism of **1** and the value of the R-factor for **2a**, see above). According to this series, the isolated molecule **2c** is characterized by the longest Si···N contact, which means that it is relatively less sensitive to the effects of the crystal field (a “harder” potential function). Note that according to [7], the more “rigid” character of the potential function of tribenzsilatrane **2c** should manifest itself in the lower sensitivity of its ¹⁵N, ²⁹Si NMR spectral properties to the nature of the solvent. Let us underline that due to the significant difference between the calculated gas-phase and experimental solid-phase geometries of **1** and **2a–c**, the patterns of change in their d_{SiN} under the influence of internal factors (the nature of X, R) may be inconsistent (Tables 2 and 3).

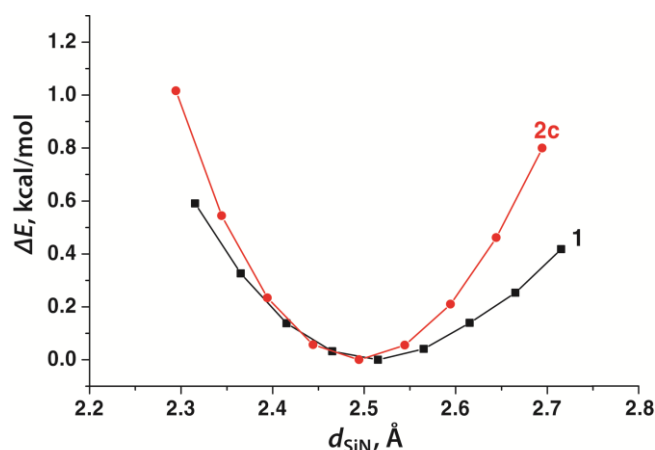


Figure 6. Potential functions of the deformation of N→Si bond in “common” silatrane Ph-Si(OCH₂CH₂)₃N **1** and in tribenzsilatrane **2c**.

Using the results of the NBO analysis, we failed to relate the increase in d_{SiN} in the series **2a**, **2b**, **2c** with the obvious difference in electronic effects in the -O-*para*-R-C₆H₃- side chains of **2a–c**, likely due to their multi-orbital structure.

Early theoretical works [2,27] have shown the N→Si bond length to depend on many factors, including the packing of silatrane molecules in crystals. Therefore, the total energy of intermolecular interactions in the crystal cell, which, as demonstrated above (see

Section 3.1), are expected to be fundamentally different for **2a**, **2b** and **2c**, should be considered as an energy criterion ΔE of the impact on the **2a–c** geometry upon their transition from the isolated state to the solid phase.

Formally, upon transition of an isolated molecule into a crystal, the structural rearrangement can occur not only towards contraction, but also towards elongation of the Si \cdots N contact. However, as has been repeatedly demonstrated in the literature (see review [27] and references therein), the increase in the dipole moment μ of the polar molecular structures containing dative bonds favors their energetically favorable deformation. In the fundamental plan, this enhances the interaction of a single molecule with its environment. In cases of **1** and **2**, only the reduction in the Si \rightarrow N bond length leads to an increase in the dipole moment μ .

For “ordinary” silatranes X-Si(OCH₂CH₂)₃N [2,46,47], a satisfactory relationship between geometric parameters of the coordination site XSiO₃N (the N \rightarrow Si bond length d_{SiN} , the displacement of the silicon atom from the equatorial plane O₃– Δ Si, the displacement of the nitrogen atom from the C₃ plane formed by the three carbon atoms associated with it, Δ N, and the degree of pentacoordination of the silicon atom, η_e) has been demonstrated for a number of examples. As d_{SiN} decreases, the coordination node deforms towards the trigonal–bipyramidal bond configuration of the central silicon atom, i.e., both the degree of pentacoordination of Si (and its planarity) and tetrahedrality of N (its maximum shift to Si) increase. A similar relationship between the parameters of the coordination site CSiO₃N with a change in d_{SiN} is also observed in the case of tribenzsilatranes **2a–c** (Table 2).

Note that in “common” silatranes **1** [44,46], the atrane cage adopts a zigzag conformation. This is not possible in molecules of **2a–c**; due to the presence of aromatic rings, the atrane cages are rigid and the torsion angles Si–O–C–C, O–C–C–N and C–C–N \rightarrow Si scarcely differ from zero (Table S1 Supplementary Materials).

4. Conclusions

Three tribenzsilatranes **2**, derivatives of 3,4,6,7,10,11-tribenzo-2,8,9-trioxa-5-aza-1-silatricyclo(3.3.3.0^{1,5})undecanes with a phenyl group at silicon and substituted at the side aromatic cycles with the *para*-R group (R = H, Me, F), have been synthesized and studied using X-ray diffractometry and DFT calculations. Like “common” silatranes **1**, their parent derivatives with OCH₂CH₂ side chains, these tribenzsilatranes have an intramolecular dative bond N \rightarrow Si whose existence is unequivocally evidenced by geometric and quantum topological (AIM) criteria and whose nature can be defined as ion-covalent. With this, the length of the N \cdots Si contact (d_{SiN}) in the crystals of tribenzsilatranes is remarkably longer than in **1**. Using DFT B3PW91/6-311++G(d,p) calculations, we have shown that this feature stems from more rigid potential functions of deformation of the N \rightarrow Si bond in **2** compared to **1**. The character (soft/hard) of the potential functions can be assessed from the difference in the calculated values of d_{SiN} in isolated molecules **2a–c** and in their crystals. Meanwhile, multiple intermolecular interactions such as the C–H \cdots π (with the aromatic rings) and C–H \cdots F types as well as of the F \cdots π type were revealed through XRD and supported by detecting *bcp*(3, –1) critical points in the quantum topological AIM analysis of these structures. These findings underline that the correct description of the structure and properties of the N \rightarrow Si bond in **2** and in their derivatives with other substituents is only possible upon careful consideration of the total energy of all intermolecular interactions in the crystal cell. Further work on the synthesis and study of the related structures is in progress.

Supplementary Materials: The following supporting information can be downloaded at: <https://www.mdpi.com/article/10.3390/cryst13050772/s1>, Figure S1: The voids in the molecular packing of **2a**; Figure S2: The voids in the molecular packing of **2b**; Figure S3: Crystal cell graph for **2c** from AIM analysis; Figure S4: The voids in the molecular packing of **2c**; Table S1: XRD Experimental and B3PW91/6-311++G(d,p) calculated (italics) selected geometric parameters of molecules **2a–c**; Figure S5: ORTEP drawing of phenylsilatrane (**1**); Figure S6: Potential functions of deformation of the N \rightarrow Si bond in “common” silatrane Ph-Si(OCH₂CH₂)₃N **1** and tribenzsilatranes **2a–c**.

Author Contributions: V.S. conceived and designed the experiments and conceptualized the work; E.D. ran the theoretical calculations and prepared the manuscript for publication; S.B. provided crystal structure analysis and reviewed and edited the manuscript; V.J. provided acquisition of funding and supervision of the research; T.R. conducted the X-ray analysis; V.R. realized the synthesis of the compounds and reviewed and edited the manuscript. All authors have read and agreed to the published version of the manuscript.

Funding: VR thanks the support from the European Regional Development Fund ERDF–Latvia (No. 1.1.1.2/VIAA/3/19/577); VJ and SB are grateful to PHC OSMOSE Project 48362YK.

Data Availability Statement: The data presented in this study are available in Supplementary Materials.

Acknowledgments: The crystal structures were obtained at the platform of X-ray diffractometry of the University of Rennes. The quantum chemistry calculations were performed within the research project of the Russian Academy of Sciences No 121021000264-1. The authors are grateful to the Irkutsk Supercomputer Center of SB RAS (<http://hpc.icc.ru/>) (accessed on 1 March 2023) for providing computational resources of the HPC-cluster “Akademik V.M. Matrosov”.

Conflicts of Interest: The authors declare no conflict of interest.

References

1. Verkade, J.G. Main group atranes: Chemical and structural features. *Coord. Chem. Rev.* **1994**, *137*, 233–295. [[CrossRef](#)]
2. Pestunovich, V.; Kirpichenko, S.; Voronkov, M. *The Chemistry of Organic Silicon Compounds*; Rappoport, Z., Apeloig, Y., Eds.; Wiley: Chichester, UK, 1998; Volume 2, pp. 1447–1537.
3. Voronkov, M.G.; Baryshok, V.P. *Use of Silatranes for Medicine and Agriculture*; Tolstikov, G.A., Ed.; Publishing House of the Siberian Branch of Russian Academy of Sciences: Novosibirsk, Russia, 2005; p. 258.
4. D'yakov, V.M.; Voronkov, M.G.; Kazimirovskaya, V.B.; Loginov, S.V.; Rasulov, M.M. *Organosilicon Chemistry VI: From Molecules to Materials*; Auner, N., Weis, J., Eds.; Wiley-VCH Verlag GmbH: Weinheim, Germany, 2008; pp. 588–594.
5. Puri, J.K.; Singh, R.; Chahal, V.K. Silatranes: A review on their synthesis, structure, reactivity and applications. *Chem. Soc. Rev.* **2011**, *40*, 1791–1840. [[CrossRef](#)] [[PubMed](#)]
6. Sidorkin, V.F.; Belogolova, E.F.; Wang, Y.; Jouikov, V.; Doronina, E.P. Electrochemical Oxidation and Radical Cations of Structurally Non-rigid Hypervalent Silatranes: Theoretical and Experimental Studies. *Chem. Eur. J.* **2017**, *8*, 1910–1919. [[CrossRef](#)]
7. Belogolova, E.F.; Sidorkin, V.F. Correlation among the Gas-Phase, Solution, and Solid-Phase Geometrical and NMR Parameters of Dative Bonds in the Pentacoordinate Silicon Compounds. 1-Substituted Silatranes. *J. Phys. Chem. A* **2013**, *117/25*, 5365–5376. [[CrossRef](#)] [[PubMed](#)]
8. Belogolova, E.F.; Liu, G.; Doronina, E.P.; Ciborowski, S.M.; Sidorkin, V.F.; Bowen, K.H. “Outlaw” Dipole-Bound Anions of Intra-Molecular Complexes. *J. Phys. Chem. Lett.* **2018**, *9*, 1284–1289. [[CrossRef](#)] [[PubMed](#)]
9. Sidorkin, V.F.; Belogolova, E.F.; Doronina, E.P.; Liu, G.; Ciborowski, S.M.; Bowen, K.H. “Outlaw” Dipole-Bound Anions of Intra-Molecular Complexes. *J. Am. Chem. Soc.* **2020**, *142*, 2001–2011. [[CrossRef](#)]
10. Belogolova, E.F.; Shlykov, S.A.; Eroshin, A.V.; Doronina, E.P.; Sidorkin, V.F. The hierarchy of ab initio and DFT methods for describing an intramolecular non-covalent Si···N contact in the silicon compounds using electron diffraction geometries. *Phys. Chem. Chem. Phys.* **2021**, *23*, 2762–2774. [[CrossRef](#)]
11. Shen, Q.; Hilderbrandt, R.L. The structure of methyl silatrane (1-methyl-2,8,9-trioxa-5-aza-1-silabicyclo(3.3.3)undecane) as determined by gas phase electron diffraction. *J. Mol. Struct.* **1980**, *64*, 257–262. [[CrossRef](#)]
12. Forgacs, G.; Kolonits, M.; Hargittai, I. The gas-phase molecular structure of 1-fluorosilatrane from electron diffraction. *Struct. Chem.* **1990**, *1*, 245–250. [[CrossRef](#)]
13. Shishkov, I.F.; Khristenko, L.V.; Rudakov, F.M.; Golubinskii, A.V.; Vilkov, L.V.; Karlov, S.S.; Zaitseva, G.S.; Samdal, S. Molecular Structure of Silatrane Determined by Gas Electron Diffraction and Quantum-Mechanical Calculations. *Struct. Chem.* **2004**, *15*, 11–16. [[CrossRef](#)]
14. Korlyukov, A.A.; Antipin, M.Y.; Bolgova, Y.I.; Trofimova, O.M.; Voronkov, M.G. Chemical bonding in the crystal structure of 1-hydrosilatrane. *Russ. Chem. Bull. Int. Ed.* **2009**, *58*, 25–30. [[CrossRef](#)]
15. Boer, F.P.; Turley, J.W.; Flynn, J.J. Structural studies of pentacoordinate silicon. II. Phenyl(2′2′,2′′-nitriлотriphenoxy)silane. *J. Am. Chem. Soc.* **1968**, *90*, 5102–5105. [[CrossRef](#)]
16. Chen, W.; Wu, G.L.; Luo, Y. *Jiegou Huaxue* (Chin.). *Chin. J. Struct. Chem.* **1987**, *6*, 165.
17. Meshgi, M.A.; Zaitsev, K.V.; Vener, M.V.; Churakov, A.V.; Baumgartner, J.; Marschner, C. Hypercoordinated Oligosilanes Based on Aminotrisphenols. *ACS Omega* **2018**, *3*, 10317. [[CrossRef](#)] [[PubMed](#)]
18. Sheldrick, G.M. *SHELXT*—Integrated space-group and crystal-structure determination. *Acta Crystallogr. Section A* **2015**, *71*, 3–8. [[CrossRef](#)] [[PubMed](#)]
19. Sheldrick, G.M. Crystal structure refinement with *SHELXL*. *Acta Crystallogr. Section C* **2015**, *71*, 3–8.
20. Frisch, M.J.; Trucks, G.W.; Schlegel, H.B.; Scuseria, G.E.; Robb, M.A.; Cheeseman, J.R.; Scalmani, G.; Barone, V.; Mennucci, B.; Petersson, G.A.; et al. *Gaussian 09, Revision C.01*; Gaussian Inc.: Wallingford, CT, USA, 2010.

21. Bader, R.F.W. *Atoms in Molecules: A Quantum Theory*; Clarendon Press: Oxford, UK, 1990; p. 458.
22. Todd, A.; Keith, T.K. *AIMAll (Version 19.02.13)*; Gristmill Software: Overland Park, KS, USA, 2019.
23. Espinosa, E.; Molins, E.; Lecomte, C. Hydrogen bond strengths revealed by topological analyses of experimentally observed electron densities. *Chem. Phys. Lett.* **1998**, *285*, 170–173. [[CrossRef](#)]
24. Espinosa, E.; Lecomte, C.; Molins, E. Experimental electron density overlapping in hydrogen bonds: Topology vs. energetics. *Chem. Phys. Lett.* **1999**, *300*, 745–748. [[CrossRef](#)]
25. Espinosa, E.; Molins, E. Retrieving interaction potentials from the topology of the electron density distribution: The case of hydrogen bonds. *J. Chem. Phys.* **2000**, *113*, 5686–5694. [[CrossRef](#)]
26. Espinosa, E.; Alkorta, I.; Rozas, I.; Elguero, J.; Molins, E. About the evaluation of the local kinetic, potential and total energy densities in closed-shell interactions. *Chem. Phys. Lett.* **2001**, *336*, 457–461. [[CrossRef](#)]
27. Korlyukov, A.A. Coordination compounds of tetravalent silicon, germanium and tin: The structure, chemical bonding and intermolecular interactions in them. *Russ. Chem. Rev.* **2015**, *84*, 422–440. [[CrossRef](#)]
28. Lyssenko, K.A.; Korlyukov, A.A.; Golovanov, D.G.; Ketkov, S.Y.; Antipin, M.Y. Estimation of the Barrier to Rotation of Benzene in the $(\eta^6\text{-C}_6\text{H}_6)_2\text{Cr}$ Crystal via Topological Analysis of the Electron Density Distribution Function. *J. Phys. Chem. A* **2006**, *110*, 6545–6551. [[CrossRef](#)] [[PubMed](#)]
29. Zhurova, E.A.; Stash, A.I.; Tsirelson, V.G.; Zhurov, V.V.; Bartashevich, E.V.; Potemkin, V.A.; Pinkerton, A.A. Atoms-in-Molecules Study of Intra- and Intermolecular Bonding in the Pentaerythritol Tetranitrate Crystal. *J. Am. Chem. Soc.* **2006**, *128*, 14728–14734. [[CrossRef](#)] [[PubMed](#)]
30. Sidorkin, V.F.; Doronina, E.P.; Belogolova, E.F. A New Approach to the Design of Neutral 10-C-5 Trigonal-Bipyramidal Carbon Compounds: A “ π -Electron Cap” Effect. *Chem. Eur. J.* **2013**, *19*, 10302–10311. [[CrossRef](#)]
31. Sidorkin, V.F.; Doronina, E.P. Cage Silaphosphanes with a P \rightarrow Si Dative Bond. *Organometallics* **2009**, *28*, 5305–5315. [[CrossRef](#)]
32. Doronina, E.P.; Sidorkin, V.F.; Lazareva, N.F. (PO \rightarrow Si) Chelates of Silylmethyl Derivatives of Phosphoric Acids R₂P(O)ZCH₂SiMe_{3-n}Hal_n ($n = 1-3$; Z = O, NMe, CH₂, S). *Organometallics* **2010**, *29*, 3327–3340. [[CrossRef](#)]
33. Sidorkin, V.F.; Belogolova, E.F.; Doronina, E.P. Assignment of photoelectron spectra of silatranes: First ionization energies and the nature of the dative Si \leftarrow N contact. *Phys. Chem. Chem. Phys.* **2015**, *17*, 26225–26237. [[CrossRef](#)]
34. Doronina, E.P.; Sidorkin, V.F.; Belogolova, E.F.; Jouikov, V. Isomer-selective dative bond O \rightarrow M (M = Si, Ge) for designing new photochromic hemi-indigo systems. *J. Organomet. Chem.* **2018**, *858*, 89–96. [[CrossRef](#)]
35. Doronina, E.P.; Jouikov, V.V.; Sidorkin, V.F. Molecular Design of Silicon-Containing Diazenes: Absorbance of E and Z Isomers in the Near-Infrared Region. *Chem. Eur. J.* **2022**, *28*, e202201508. [[CrossRef](#)]
36. Reed, A.E.; Curtiss, L.A.; Weinhold, F. Intermolecular interactions from a natural bond orbital, donor-acceptor viewpoint. *Chem. Rev.* **1988**, *88*, 899–926. [[CrossRef](#)]
37. Glendening, E.D.; Badenhoop, J.K.; Reed, A.E.; Carpenter, J.E.; Bohmann, J.A.; Morales, C.M.; Weinhold, F. *NBO 5.G*; Theoretical Chemistry Institute, University of Wisconsin: Madison, WI, USA, 2004. Available online: <https://nbo7.chem.wisc.edu/> (accessed on 20 March 2023).
38. Granovsky, A.A. Firefly Version 8. Available online: <http://classic.chem.msu.su/gran/firefly/index.html> (accessed on 20 March 2023).
39. Tamao, K.; Hayashi, T.; Ito, Y.; Shiro, M. Pentacoordinate anionic bis(siliconates) containing a fluorine bridge between two silicon atoms. Synthesis, solid-state structures, and dynamic behavior in solution. *Organometallics* **1992**, *11*, 2099–2114. [[CrossRef](#)]
40. Frye, C.L.; Vincent, G.A.; Hauschildt, G.L. Pentacoordinate Silicon Derivatives. III.1 2,2',2''-Nitrilotriphenol, a New Chelating Agent. *J. Am. Chem. Soc.* **1966**, *88*, 2727–2730. [[CrossRef](#)]
41. Olsson, L.; Ottosson, C.-H.; Cremer, D. Properties of R₃SiX Compounds and R₃Si⁺ Ions: Do Silylium Ions Exist in Solution? *J. Am. Chem. Soc.* **1995**, *117*, 7460–7479. [[CrossRef](#)]
42. Ottosson, C.-H.; Cremer, D. Intramolecularly Stabilized Phenylsilyl and Anthrylsilyl Cations. *Organometallics* **1996**, *15*, 5309–5320. [[CrossRef](#)]
43. Turley, J.W.; Boer, F.P. Structural Studies of Pentacoordinate Silicon. I. Phenyl-(2,2',2''-nitrilotriethoxy)silane. *J. Am. Chem. Soc.* **1968**, *90*, 4026–4030. [[CrossRef](#)]
44. Parkanyi, L.; Simon, K.; Nagy, J. Crystal and Molecular Structure of β -l-Phenylsilatrane, C₁₂H₁₇O₃NSi. *Acta Cryst.* **1974**, *30*, 2328–2332. [[CrossRef](#)]
45. Parkanyi, L.; Nagy, J.; Simon, K. Crystal and Molecular Structure of γ -l-Phenylsilatrane, Some Structural Features of Silatranes. *J. Organomet. Chem.* **1975**, *101*, 11–18. [[CrossRef](#)]
46. Pestunovich, V.; Lukevics, E.; Pudova, O.; Sturkovich, R. *Molecular Structure of Organosilicon Compounds*; John Wiley: Chichester, NY, USA, 1989; p. 359.
47. Greenberg, A.; Wu, G. Structural Relationships in Silatrane Molecules. *Struct. Chem.* **1990**, *1*, 79–85. [[CrossRef](#)]

Disclaimer/Publisher’s Note: The statements, opinions and data contained in all publications are solely those of the individual author(s) and contributor(s) and not of MDPI and/or the editor(s). MDPI and/or the editor(s) disclaim responsibility for any injury to people or property resulting from any ideas, methods, instructions or products referred to in the content.